Applied Catalysis B: Environmental 84 (2008) 803–812

Contents lists available at ScienceDirect

Applied Catalysis B: Environmental

journal homepage: www.elsevier.com/locate/apcatb

Global kinetic modelling of the reaction of soot with O_2 and NO_x on Fe_2O_3 catalyst

D. Reichert, T. Finke, N. Atanassova, H. Bockhorn, S. Kureti *

Institut für Technische Chemie und Polymerchemie, Universität Karlsruhe, Kaiserstrasse 12, D-76128 Karlsruhe, Germany

ARTICLE INFO

Article history:
Received 29 April 2008
Received in revised form 17 June 2008
Accepted 18 June 2008
Available online 24 June 2008

Keywords:
Direct conversion
Diesel
Soot
Soot oxidation
NO reduction
Fe_2O_3
Catalyst
Mechanism
Kinetic modelling
Active sites

ABSTRACT

This study deals with the catalytic reaction of NO_x and soot on Fe_2O_3 to yield N_2 and CO_2 in excess of oxygen. Based on the three types of kinetic experiments, i.e. temperature programmed oxidation (TPO), transient examinations and gradient-free loop reactor experiments, as well as mechanistic studies presented recently a global kinetic model is established. The model includes catalytic effect of the iron oxide on soot/O_2 reaction, whereas it is assumed that NO_x reduction occurs on the soot without direct participation of Fe_2O_3. Furthermore, the model implies global kinetic expressions for the CO_x formation and NO_x reduction. These equations include the evolution of the surface area of soot and the correlation of reactive carbon sites (C_f) with those specifically involved in NO_x reduction (C^*). The kinetic model is sequentially developed by accounting for the catalytic and non-catalytic soot/O_2 as well as soot/NO_x/O_2 conversion. Kinetic parameters are taken from the literature and are also determined from a fit to experimental data. Comparison of measured and calculated data shows accurate reproduction of the experiments and the model. Finally, the kinetic model is validated by some simulations.

1. Introduction

Diesel engines with direct fuel injection reveal the highest efficiency for mobile applications resulting in reduced fuel consumption and CO_2 production. However, a constraint of diesel engines is the emission of nitrogen oxides (NO_x) and soot. In the past much attention has been concentrated on the catalytic removal of these pollutants from the oxygen rich diesel exhaust, mainly dealing with the diminution of either soot or NO_x [1,2]. A technique for combined removal of both pollutants called DPNR (diesel particulate NO_x reduction) has been presented recently [3]. This system involves improved internal combustion and a specific after treatment unit which consists of a particulate filter coated with a NO_x storage reduction catalyst [4]. As a unique feature DPNR is claimed to provide soot oxidation even under rich conditions. However, despite of the intensive activities in research and development the direct catalytic conversion of soot and NO_x into N_2 and CO_2 has hardly been taken into in account [5–8].

Examinations on the reaction of soot with NO_x and O_2 identify the NO_x reduction to be a side reaction of the soot/O_2 conversion [9–11]. In the first reaction step carbon is oxidised by O_2 leading to surface oxygen compounds (SOC) [12]. Their decomposition results in the evolution of gaseous CO_x and formation of coordinatively unsaturated carbon atoms that represent the reactive sites (C_f) in soot oxidation. However, for the adsorption of NO and formation of N_2 a certain surface configuration of C_f sites is required. Those sites subsequently denoted as C^* reveal adequate orientation of the molecule orbitals leading to the dissociative adsorption of NO and production of five or six membered rings with C(O) and C(N) sequences (Fig. 1). Another NO molecule adsorbs on a C(N) group to form a cyclic (CONNC) system, for instance a six membered C_3N_2O ring [9,13]. Thermal decomposition results in the release of N_2 and CO, whereby a surface situation of carbon sites is produced that is different from the initial one. Thus, the N_2 formation ceases. However, in presence of O_2 the active surface configuration can be restored as shown in Fig. 1.

The catalytic effect of Fe_2O_3 in soot/NO_x/O_2 reaction is to enhance the oxygen transfer to the soot thus boosting the formation of C_f and C^* sites. Nevertheless, Fe_2O_3 does not directly affect the NO_x reduction to N_2 [9,14].

* Corresponding author. Tel.: +49 721 608 8090; fax: +49 721 608 2816.
E-mail address: kureti@ict.uni-karlsruhe.de (S. Kureti).

0926-3373/$ – see front matter © 2008 Elsevier B.V. All rights reserved.
doi:10.1016/j.apcatb.2008.06.014

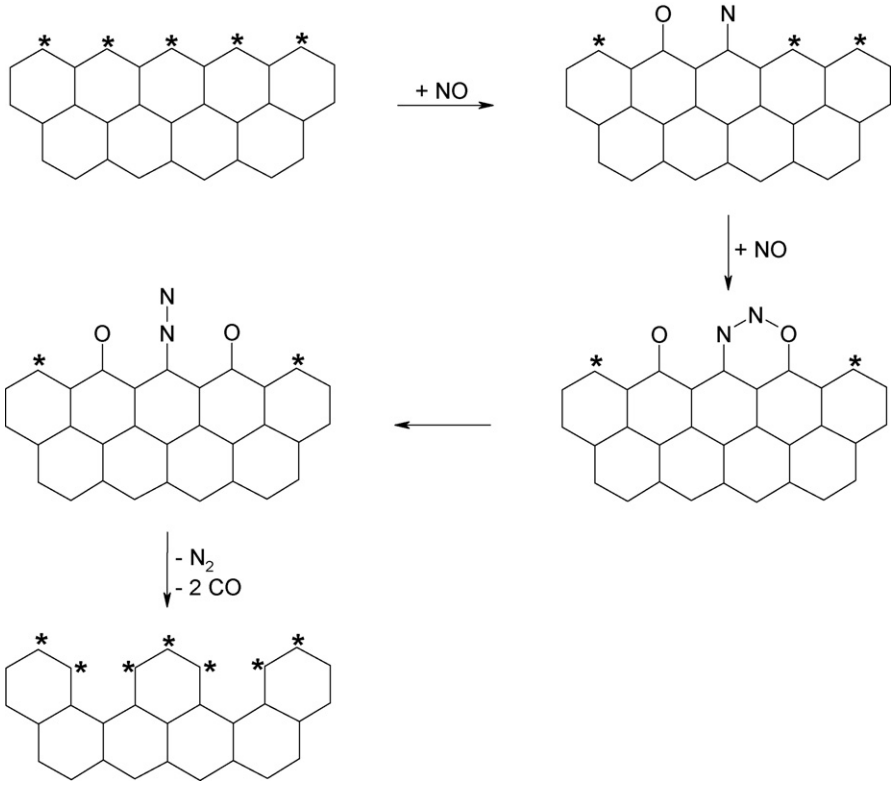

Fig. 1. Postulated mechanism of the soot/NO_x/O_2 reaction [9,13]. The edge C atoms on the upper side are unsaturated that is indicated by the asterisk, while the other C atoms are terminated with H atoms; the C body is polyaromatic.

Numerous studies have been reported on the reaction of carbon black and NO_x in the absence of O_2. The mechanistic suggestions are in fair agreement with the one postulated above for the presence of oxygen involving dissociation of NO as well as formation of C(O) and C(N) species which lead to the production of N_2 [15].

The oxidation of soot includes a very complex network of elementary reactions which is mainly related to the large heterogeneity of the soot surface, i.e. the nature of active carbon sites and surface compounds formed. Thus, the kinetics of soot oxidation is widely expressed by global approaches, i.e. potential rate laws [16–18]. Indeed, it has been shown that the kinetics of the soot/O_2 reaction can be reliably described by power law models if the distribution of the activation energy of adsorption or desorption is broad [19]. In Eq. (1) a corresponding rate law is defined for the CO_x evolution including the rate constant k_{CO_x}, the amount of the C_f sites ($n(C_f)$) and the gas-phase concentration of oxygen ($c(O_2)$) with its respective reaction order (n_{O_2}).

$$r(CO_x) = k_{CO_x} n(C_f) c(O_2)^{n_{O_2}} \quad (1)$$

The connection between number of C_f sites and soot morphology, e.g. absolute surface area ($S(X)$) that changes with soot conversion (X), can be simply described by Eq. (2); λ represents the surface concentration of C_f sites.

$$n(C_f) = \lambda S(X) \quad (2)$$

Some empirical models have been reported to express the dependence of the surface area from soot conversion. A very prominent one is the shrinking core model [20] and the pore models from Bhatia and Perlmutter [21] and Reyes and Jensen [22].

In contrast to soot/O_2 conversion, the soot/NO reaction implies specific C^* sites which are a subset of the C_f atoms. Following Eq. (1) the global rate of NO consumption $r(NO)$ is defined by Eq. (3), wherein k_{NO} is the rate constant, $n(C^*)$ the amount of C^* sites depending on the soot conversion, $c(NO)$ the NO concentration and n_{NO} the reaction order of NO.

$$r(NO) = k_{NO} n(C*) c(NO)^{n_{NO}} \quad (3)$$

The objective of the present study is the construction of a global kinetic model for the catalytic soot/NO_x/O_2 reaction on Fe_2O_3. The kinetic model is based upon the mechanism described in Fig. 1 [9] and is fitted to a series of experimental temperature programmed oxidation (TPO) investigations. Due to the complexity of the reaction system a sequential approach is pursued starting from the non-catalytic soot/O_2 conversion. To decrease the number of free parameters in the fitting procedure some kinetic parameters are determined by independent experiments, while others are taken from the literature.

2. Experimental

2.1. Preparation and characterisation of the Fe_2O_3 catalyst and soot

The α-Fe_2O_3 catalyst is prepared by polyvinyl alcohol method [7] with final calcination in air at 650 °C. The crystalline structure is confirmed by PXRD (Siemens, D 500), while multipoint BET (Sorptomatic 1990, Porotec) indicates a specific surface area of 15 m^2/g.

The soot is prepared by burning a C_3H_6/O_2 mixture in a diffusion flame and is separated from the exhaust by employing a particulate filter as reported recently [23]. The most important physical–chemical properties of the soot collected are briefly summarised in Table 1.

Table 1
Physical–chemical properties of the used C_3H_6 soot

BET surface area	91 m^2/g
Amount of adsorbed species	2.6 wt.%
Chemical composition[a,b]	98.8 wt.% C, 0.7 wt.% O, 0.5 wt.% H
Diameter of primary particles	20–100 nm

[a] The amount of adsorbed species is neglected.
[b] The soot is ashless.

2.2. Modification of the soot by O_2 exposure

To investigate the evolution of the BET surface area with increasing soot conversion TPO experiments are performed with fresh soot (1.00 g). The preparation of the soot granules used is described in Section 2.3. In TPO, the soot is oxidised to a level of 25, 50 and 75%, respectively. This treatment is carried out on a laboratory bench which is equipped with a quartz glass tube reactor (i.d. 38 mm). The soot is exposed to a gas mixture of 6 vol.% O_2 and 94 vol.% Ar (500 ml/min, STP) and temperature is linearly increased from 150 °C with a rate of 1.5 K/min. When the intended conversion is reached, the reaction is quenched by stopping the O_2 flow. After this, it is rapidly cooled down to room temperature. Soot conversion is determined by continuously integrating the traces of CO and CO_2 which are monitored by non-dispersive infrared spectroscopy (NDIR, Uras 10E, Hartmann & Braun). The specific surface area of the soot samples is measured by multipoint BET.

The content of SOC species originated from O_2 exposure is analysed by temperature programmed desorption (TPD). Here, the oxidised soot (0.12 g) is linearly heated in another quartz glass tube (i.d. 8 mm) from room temperature to 1000 °C in a N_2 flow (F) of 500 ml/min (STP); the heating rate is kept at 10 K/min.

The development of BET surface area of the soot present in the catalytic mixture is also evaluated at 25, 50 and 75% conversion. After respective O_2 exposure the mixture is treated with concentrated HCl for 24 h at 70 °C to dissolve the Fe_2O_3 catalyst. A blank experiment with pure soot shows that HCl treatment does not change the BET surface area. Finally, the remaining mass is washed several times with deionised water. However, as proven by PXRD and thermogravimetric analyses (Netzsch, STA 409) carried out in synthetic air the residual still reveals iron corresponding to 5–15 wt.% Fe_2O_3. Accumulation of iron species on the soot surface is confirmed by a blank experiment in which soot is treated with $FeCl_3$ solution followed by intense washing and TG analysis. It is therefore inferred that the BET surface area of the soot present in the catalytic mixture cannot be determined reliably.

2.3. Kinetic studies

For the catalytic studies the Fe_2O_3 catalyst is blended with soot in the weight ratio of 27 corresponding to a molar ratio of 2. The blending is accurately performed by grinding the solids in a mortar that results in tight contact. To avoid discharge in the measurements the mixture is pelletised at 40 MPa, granulated and sieved to a mesh size of 125–250 and 250–500 μm; the former size is taken for TPO, while the latter is used for experiments in the loop reactor. Preliminary tests demonstrate that pressing and granulating does not affect the activity of the mixture, whereas the initial grinding is found to be the crucial step in preparation. The tight contact mode is generally considered to be less representative for soot deposited in particulate filters, but it is suitable for the intended basic examinations as reproducible conditions are simply provided. For reference purposes pure soot granules are also made. They are prepared in the same way as described for the catalytic mixture.

Furthermore, in TPO as well as loop reactor measurements small differences between inlet and outlet temperatures (<10 K) are observed, even at maximum oxidation rates. Hence, for simplicity only the outlet temperature will be noted throughout this paper.

2.3.1. TPO studies

The TPO examinations represent the experimental base for both fitting calculations and validation of the kinetic model. The TPO studies have recently been reported in detail in this journal [9] and therefore only a brief description is given here. For non-catalytic conversion 0.12 g soot granules diluted with 0.50 g crushed quartz wool is taken, whereas in the catalytic experiments a mixture of 3.197 g catalyst and 0.12 g soot is employed. The feed gas consists of 0 or 500 ppm NO, 6 vol.% O_2 and Ar as balance (500 ml/min, STP), while temperature is linearly increased from 150 °C with a rate of 1.5 K/min. The effluents are analysed as follows: CO, CO_2 and N_2O by NDIR (Uras 10E, Hartmann and Braun), N_2 by gas chromatography coupled with thermal conductivity detection (GC/TCD RGC 202, Siemens), NO_x by chemiluminescence (CLD EL-ht, Eco Physics) and O_2 by magnetomechanics (Magnos 6 G, Hartmann und Braun).

2.3.2. Studies in the gradient-free loop reactor

To obtain independent kinetic parameters the kinetics of the soot/O_2 reaction being the dominating reaction in catalytic as well as non-catalytic soot/NO_x/O_2 conversion is examined separately. For this purpose a gradient-free loop reactor (quartz glass tube, i.d.: 10 mm) with external gas cycle is used; as circulation pump a MZ2C from Vacuubrand is employed. Tracer experiments show that this reactor approaches satisfactorily the residence time profile of the ideal continuously stirred tank reactor thus excluding significant concentration gradients. The total volume flow is 290 ml/min (STP) with a recycle ratio Ψ ($\Psi = \text{flow}_{\text{loop}}/\text{flow}_{\text{out}}$) of 145 corresponding to differential soot conversion in the volume elements passing the reactor. This results in isothermal conditions as indicated above. Moreover, since variation of Ψ (90–145) and size of soot granules (125–500 μm) does not show a significant change in CO_x production rate the effect of film and pore diffusion is experimentally excluded. Additionally, mass transfer limitations are also estimated by Mears [24] and Weisz criteria [24,25] confirming the experimental result.

In the non-catalytic investigations the soot granules (24 mg) are diluted with crushed quartz wool (476 mg) to avoid hot spots and to reduce the back pressure (bed length: 12 mm), while for the catalytic studies a blend of 160 mg Fe_2O_3 and 6 mg soot is taken (bed length: 2 mm). The catalyst/soot mixture is not blended with quartz wool as the dilution would lead to an increase in back pressure due to the high mass of catalyst. In the reactor, each sample is fixed with quartz wool. The bed is held downstream by a cordierite honeycomb (cell density: 200 cpsi; d: 9 mm; l: 15 mm) which itself is fixed by the outlet thermocouple located 25 mm behind the sample. Preliminary investigations show no effect of the cordierite monolith on inlet and outlet temperature. Inlet temperature is measured 10 mm in front of the bed. In the experiments, N_2 is firstly dosed, then the cycle pump is switched on and temperature is raised. After the intended temperature is reached, O_2 (6 vol.%) is supplied and the reactor effluents are monitored by NDIR (Binos 4b.1 for CO_2; Binos 1.2 for CO, both analysers from Leybold–Heraeus). For comparison purposes the catalytic (250–380 °C) and non-catalytic reaction (290–430 °C) is investigated in a very similar temperature range.

3. Results and discussion

3.1. Kinetics of the decomposition of SOC species

To estimate the activation energy for the decomposition of surface oxygen compounds TPD profile of soot is numerically

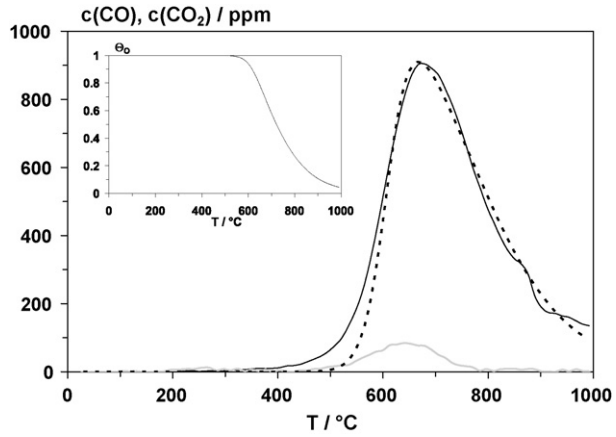

Fig. 2. Experimental profile of CO (–) and CO_2 (▬) in TPD of soot preliminarily oxidised up to 75% and calculated trace of CO (- - -). The inset shows the calculated development of coverage of SOC. *Conditions*: m(soot) = 0.12 g, m(quartz wool) = 0.50 g, $F(N_2)$ = 500 ml/min, β = 10 K/min; preliminary O_2 exposure is described in Section 2.2.

modelled. For this purpose soot preliminary oxidised up to 75% is exemplarily taken. The corresponding TPD pattern (Fig. 2) is representative for the remaining soot samples (Section 2.2) indicating a rather weak CO_2 peak at about 660 °C and an approximately 10 times stronger release of CO with a maximum at ca. 680 °C. This product distribution is in line with results from Chambrion et al. [26]. Since the desorption of CO_2 is a minor pathway, the release of CO is considered in the numerical modelling exclusively. In the model the surface oxygen compounds (C(CO)) are supposed to be equivalent, whereby the decomposition is expressed by Eq. (4). Approximation of equivalent surface species is widely accepted as effective method to describe gas–solid interactions [27,28] and is also reported for the chemisorption of oxygen on carbon [29]. As another supposition the kinetic model neglects the readsorption of CO, i.e. the potential backward reaction of Eq. (4).

$$C(CO) \rightarrow C_f + CO(g) \tag{4}$$

Kinetics of CO desorption is defined by Eq. (5) representing an Arrhenius based rate expression; A_{des} is the pre-exponential factor, $E(0)$ the activation energy at zero coverage and θ_O is the coverage of SOC. Due to repulsion of the SOC species linear decrease in activation energy with increasing oxygen coverage is assumed [28,30]. For this purpose the constant α is introduced, which also reflects the heterogeneity of the soot surface [27].

$$r_{des} = A_{des} \exp\left(-\frac{E(0)(1-\alpha\theta_O)}{RT}\right)\theta_O^{3.3} \tag{5}$$

To reduce the number of fitting parameters A_{des} (10^{13} s^{-1}) is adopted from the literature [31] and the initial surface coverage is assumed to be unity being in good agreement with Ahmed and Back [32]. Furthermore, the reaction order (θ_O = 3.3) is taken from Reichert who determined this parameter for the present soot by the differential method [33]; it has to be mentioned that this constant is not a fundamental one and might be problematic when extrapolated to other temperature regimes and different types of soot.

The numerical modelling is based upon the combination of the mass balance of gas-phase (Eq. (6)) and adsorbed oxygen containing species (Eq. (7)) resulting in a system of an algebraic (Eq. (8)) and a non-linear differential equation (Eq. (9)). In these equations V represents the volume of the soot derived from its initial density (2.0 g/cm^3) [34,35] and β is the heating rate. Furthermore, in Eq. (6) the plug flow reactor used is described by the model of the continuously stirred tank reactor. This approach has been shown to be a good approximation and is frequently applied in TPD modelling [36,37]. The surface coverage depending on the temperature is calculated by using the Matlab tool ods15s, while the free parameters, i.e. $E(0)$ and α, are estimated with Isqcurvefit (Matlab).

$$Fc_{CO(g),in} - Fc_{CO(g),out} + Vr_{des} = 0 \tag{6}$$

$$V\frac{d\theta_O}{dt} = -r_{des} \tag{7}$$

$$c_{CO(g)} = \frac{VA_{des}\exp(-E_2(0)(1-\alpha_2\theta_O)/RT)\theta_O^{3.3}}{F} \tag{8}$$

$$V\beta\frac{d\theta}{dT} = -A_{des}\exp\left(-\frac{E_2(0)(1-\alpha_2\theta_O)}{RT}\right)\theta_O^{3.3} \tag{9}$$

The estimation procedure leads to an activation energy for the CO desorption of 310 ± 1 kJ/mol, whereas α is determined to be 0.121 ± 0.002; the errors refer to the 95% confidence interval indicating high reliability. The activation energy calculated is a typical one for the desorption of SOC. Literature data range from 110 to 400 kJ/mol [19,38–40], whereupon release of CO_2 necessitates lower activation energy than for CO [41]. The constant α is relatively high being in line with the heterogeneity of the soot surface, e.g. for the Fe_2O_3 catalyst used α amounts to 0.0015 only [30].

The profile of the SOC coverage calculated is displayed in the inset of Fig. 2 obviously decreasing with temperature. Finally, Fig. 2 evidences that the experimental TPD curve is well fitted by the kinetic data implemented in the SOC decomposition model.

3.2. Kinetics of the catalytic and non-catalytic soot/O_2 reaction

Typical data of the kinetic studies in the loop reactor are exemplarily demonstrated for the soot/O_2 reaction performed at 430 °C (Fig. 3). The soot oxidation always shows a maximum of CO_x followed by a continuous decline, i.e. a steady state is never observed, even with varying experimental parameters (Ψ, F, m). From the CO_x traces which correspond to conversions between 10 and 30% the rate of soot oxidation is derived as there the concentration of carbon oxides is measured reliably (Eq. (10)); V_m

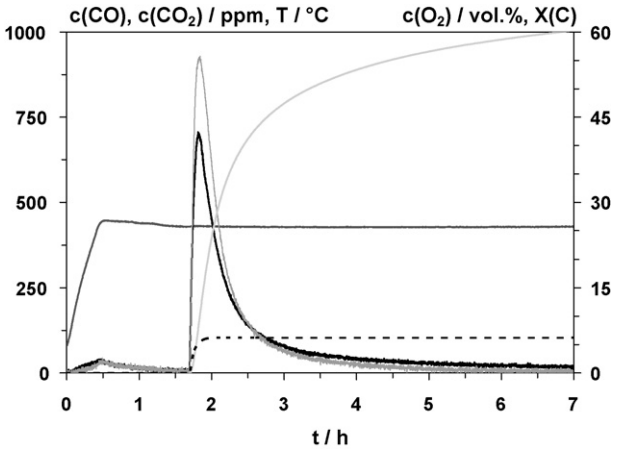

Fig. 3. Profile of O_2 (- - -), CO_2 (–), CO (▬), soot conversion (▬) and temperature (—) in non-catalytic soot/O_2 reaction carried out in the loop reactor. *Conditions*: m(C) = 24 mg (diluted with 476 mg quartz wool), $c(O_2)$ = 6 vol.%, $c(N_2)$ = 94 vol.%, F = 290 ml/min (STP), T = 430 °C, Ψ = 145.

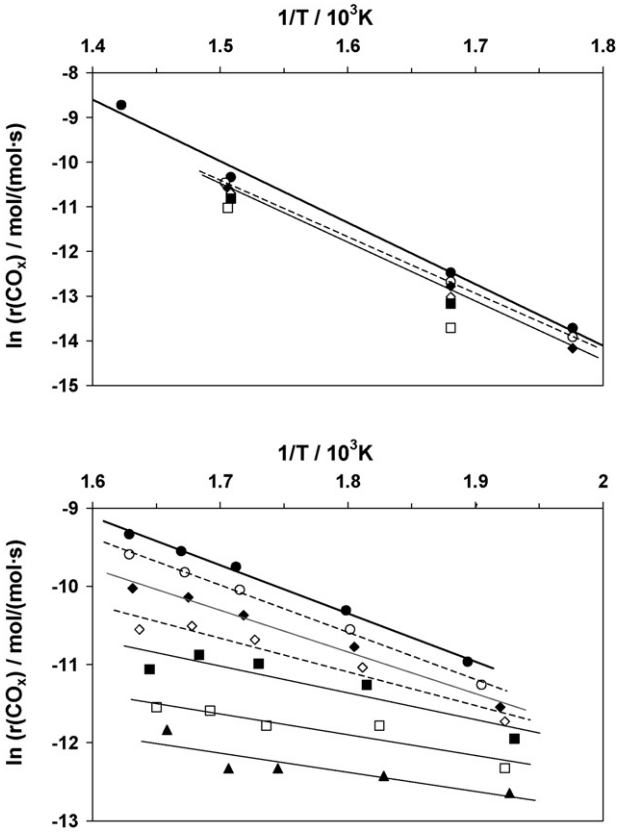

Fig. 4. Arrhenius plot of $r(CO_x)$ for catalytic (bottom) and non-catalytic soot/O_2 reaction (top); the symbols represent soot conversions of 10% (●), 12.5% (○), 15% (◆), 17.5% (◇), 20% (■), 25% (□) and 30% (▲). Conditions are described in Section 2.3.2.

is the molar volume at 20 °C and n_0 the initial molar amount of soot.

$$r(CO_x) = \frac{(c(CO) + c(CO_2))FV_m}{n_0} \quad (10)$$

The catalytic soot oxidation indicates a very similar CO_x profile as compared to the non-catalytic reaction, whereas CO is detected in rather low concentrations only. This effect is associated with the high CO oxidation activity of the Fe_2O_3 catalyst [9]. As no steady state appears in catalytic as well as non-catalytic soot/O_2 reaction the kinetic data are analysed in a particular fashion, that is the rates of a certain conversion level obtained at different temperatures are summarised and plotted in an Arrhenius diagram (Fig. 4). Apparent activation energy (E_A) is then deduced from the slope of the regression lines; error propagation of the least square fitting is less than 10%. Fig. 5 shows that the overall activation energy of the non-catalytic soot/O_2 reaction amounts to ca. 115 kJ/mol (X = 10.15%), while for the catalytic conversion it is found to be significantly lower (<56 kJ/mol). This difference evidences the enhancing effect of the Fe_2O_3 catalyst [9]. However, in presence of the catalyst the apparent activation energy decreases with soot conversion from 56 kJ/mol (X = 10%) to approx. 20 kJ/mol (X = 30%).

We have recently reported that the Fe_2O_3 catalyst acts as an oxygen pump which continuously transfers oxygen from the gas-phase via its surface to the soot [9]. The oxygen transfer occurs at the contact points of both solids and is maintained up to high conversion levels. This release of oxygen produces vacancies on the Fe_2O_3 that are refilled by neighboring surface oxygen leading to a kind of cascade of formation and refilling of surface vacancies. Finally, vacancies produced in a certain distance to the contact points are refilled by gas-phase oxygen. It has been shown that the

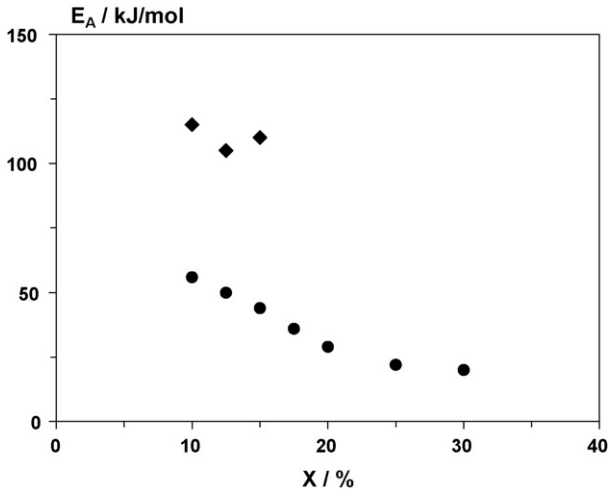

Fig. 5. Apparent activation energy of non-catalytic (◆) and catalytic soot/O_2 reaction on Fe_2O_3 (●) as function of soot conversion; the values of E_A are obtained from the Arrhenius plot depicted in Fig. 4.

dissociative adsorption of O_2 on Fe_2O_3 reveals an activation energy which is very close to 0 kJ/mol, whereas thermal desorption necessitates an activation energy of about 193 kJ/mol [30]. It is therefore concluded that adsorption and desorption of oxygen does not represent the rate-determining step in catalytic soot/O_2 reaction. Moreover, for surface diffusion on solids it is generally accepted that the activation energy is in the order of 10–20% of the binding energy of the adsorbate [42]. As the adsorption enthalpy of O_2 on Fe_2O_3 is reported to be ca. 120 kJ/mol, we estimate the activation energy of surface diffusion to be in the range of ca. 10–25 kJ/mol [43]. These values are very similar to the apparent activation energy determined above. Thus, it is assumed that the surface diffusion of oxygen is the rate-determining step of soot/O_2 reaction on Fe_2O_3 when carried out under isothermal conditions. Furthermore, it is speculated that the decrease in activation energy refers to the adsorption of CO_2 on the catalyst. It is well-known that in CO_2 adsorption on oxide surfaces carbonato species are produced, in which the carbonate ligand is coordinated to one or two Lewis acid Fe^{3+} sites representing oxygen vacancies [30]. Thus, the formation of these carbonato complexes should immediately cause the inhibition of surface diffusion of oxygen.

The comparison of the activation energy of soot oxidation determined in present work with literature data is difficult as the kinetic parameters strongly depend on numerous factors, for instance the type of carbonaceous material, its production conditions and reaction temperature. In general, the activation energy of soot/O_2 reaction decreases in the order: soot > activated carbon > chars > graphite [16]. For the oxidation of soot below 700 °C apparent activation energies of ca. 100–210 kJ/mol are reported [16,18,34,44,45]. Thus, present value of 115 kJ/mol is in the lower range of the reference data.

For chemisorption of O_2 on model graphites density functional theory calculations indicate activation energies ranging from 0 to about 30 kJ/mol [46–48]. Regarding the formation of SOC species, the production of two separated ketone groups is reported to show an activation energy of 19 kJ/mol. Subsequent rearrangement to a stable lactone followed by formation of a ketene and then a diketone is found to be 108, 154 and 119 kJ/mol, respectively [47]. Furthermore, Feng and Bhatia indicate by experiment that the activation energy on a char and a resin increases with growing coverage; i.e. from 40 to 120 kJ/mol for the first and from 5 to 35 for the latter [29]. Taking the activation energy as a tool for the assignment of the rate-determining step we suppose that the

formation of surface oxygen compounds is limiting the soot/O_2 reaction; contrary, the desorption of SOC is excluded as the determining step as it reveals a much higher activation energy (310 kJ/mol) as shown in Section 3.1.

3.3. Evaluation of the number of reactive carbon sites in soot/O_2 reaction

As demonstrated in Eq. (1), the rate of CO_x formation is considered to depend on the number of C_f sites which is deduced from the surface concentration λ and the absolute surface area of the soot ($S(X)$; Eq. (2)). The evolution of the relative surface area ($S(X)/S_0$) with proceeding conversion firstly increases, goes through a maximum and declines finally (Fig. 6). This development is satisfactorily described neither by the shrinking core nor the random pore model, whereas the latter reveals a much better approximation. Hence, we empirically advance the formula from Bhatia [21] by implementing the factor f and the exponent $1/q$ (Eq. (11)); with $f = 300$ and $q = 3$ the experimental data are described well as shown in Fig. 6.

$$\frac{S(X)}{S_0} = (1 - X)(1 + fX)^{1/q} \tag{11}$$

$S(X)$ is simply calculated from the BET surface area and the mass of soot ($m(X)$, Eq. (12)) remaining in oxidation.

$$m(X) = m_0(1 - X) \tag{12}$$

In accordance with literature [32] the surface concentration of the C_f sites is estimated by TPD. λ is then obtained by coupling the amount of CO_x released and the mass of soot with BET surface area. It is obvious that this approach is a rather rough approximation which involves the following assumptions: (a) each desorbed CO_x molecule leads to the formation of one C_f site; (b) the production of H_2O in TPD is not considered to produce C_f sites; (c) the number of CO_x desorbed directly after the O_2 pretreatment is neglected; (d) in soot oxidation present SOC species desorb to form C_f sites.

The total amount of CO_x, respective BET surface area (S_{BET}) and resulting surface concentration of SOC species of fresh and pretreated soot samples are summarised in Table 2. From the assumptions stated above a very similar surface concentration of C_f sites is inferred regardless of the pretreatment of the sample; the average value of λ is 8.7 μmol/m^2. This result is in the same order of magnitude as reported by Ahmed amounting to 18–57 μmol/m^2 [32].

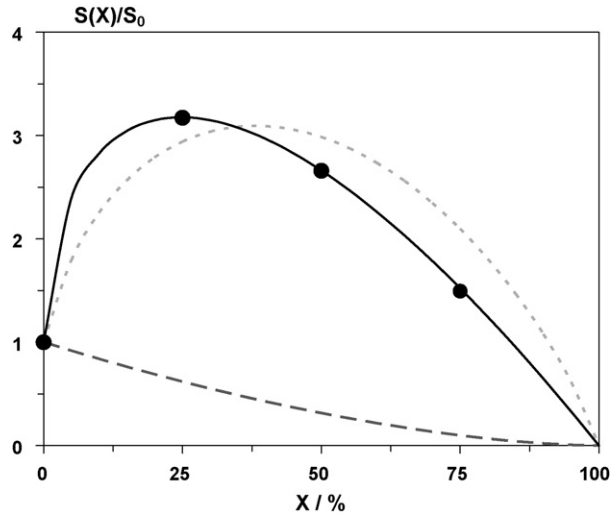

Fig. 6. Evolution of $S(X)/S_0$ with proceeding conversion of soot; experimental data (●) are compared with the shrinking core model (- - -), random pore model from Bhatia ($\alpha = 50$; - - -) and the empirical model defined by Eq. (11) (—).

Table 2
BET surface area and total amount of SOC species of the soot samples oxidised to specific conversion levels; preliminary O_2 exposure is described in Section 2.2

	X (%)			
	0	25	50	75
S_{BET} (m^2/g)	91	385	484	544
$n(CO_x)$ (mmol/g)	0.86	3.73	3.88	4.24
$n(CO_x)$ (μmol/m^2)	9.4	9.7	8.0	7.8

3.4. Global kinetic modelling of the catalytic and non-catalytic soot/O_2 reaction

In the TPO studies the time dependent soot conversion ($X(t)$) is amenable by integration of the molar flux of CO_x evolved (Eq. (13)). Furthermore, temperature is a linear function of time (Eq. (14)).

$$X(t) = \frac{1}{n_0}\int_0^t c(CO_x)F\,dt \tag{13}$$

$$T = T_0 + \beta t \tag{14}$$

Then, the rate of CO_x formation is defined by subsequent non-linear differential equation (Eq. (15)); T_0 is set 0 K.

$$r(CO_x) = n_0\beta\frac{dX}{dT} \tag{15}$$

By combining Eq. (1) with Eqs. (2), (11) and (12) and describing k_{CO_x} with an Arrhenius expression, that includes the pre-exponential factor A_{CO_x} and the apparent activation energy E_{A,CO_x}, the global rate of catalytic and non-catalytic soot/O_2 reaction is described as follows:

$$n_0\beta\frac{dX}{dT} = A_{CO_x}\,e^{(-E_{A,CO_x}/RT)}\lambda S_0 m_0(1 - X)(1 + fX)^{1/q}c(O_2)^{n_{O_2}} \tag{16}$$

Eq. (16) is solved numerically by Matlab tool rk8fixed.m using a Runge–Kutta algorithm. The fitting calculations are performed with the Matlab function leasqr.m. Since Eq. (16) represents a global rate law, a specific reactor model is not implemented as compared to TPD modelling (Section 3.1).

For the catalytic conversion λ, f and q are adopted from the non-catalytic reaction. Additionally, with the exception of the different pathways of chemisorption of oxygen our model includes the same mechanism of soot oxidation and change in morphology in absence and presence of the Fe_2O_3 catalyst. Experimental confirmation of the development of surface area and number of C sites with soot conversion was not practicable with catalyst as reported in Section 2.2.

In accordance with literature the apparent reaction order of O_2 is assumed to be 1 [18]. Additionally, for the non-catalytic soot/O_2 reaction the apparent activation energy is taken from the loop reactor studies. A_{CO_x} is kept as free parameter which is estimated by a non-linear regression method. The result of the calculations is shown in Fig. 7 indicating satisfactory description of the TPO profile of soot/O_2 conversion; the including parameters as well as the correlation coefficient (R^2) are listed in Table 4.

In presence of the Fe_2O_3 catalyst the soot oxidation is significantly enhanced (Fig. 8), for instance the peak concentration of CO_2 is shifter ca. 160 K to lower temperatures. This is in agreement with related studies [9] and substantiates the kinetic

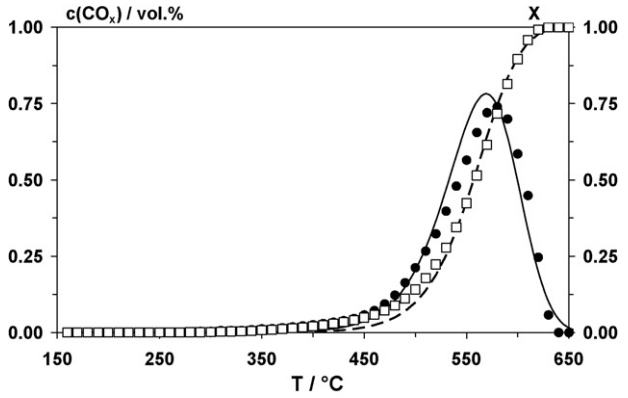

Fig. 7. Comparison of experimental and fitted CO_x concentration (●, —) and soot conversion (□, - - -) in non-catalytic soot/O_2 reaction; symbols represent experimental data. Conditions and kinetic parameters are listed in Table 4.

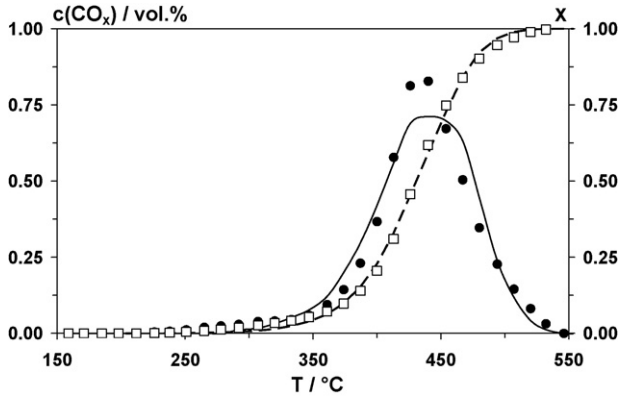

Fig. 8. Comparison of experimental and fitted CO_x concentration (●, —) and soot conversion (□, - - -) in catalytic soot/O_2 reaction on Fe_2O_3; symbols represent experimental data. Conditions and kinetic parameters are listed in Table 4.

studies performed in the loop reactor (Section 3.1), where E_{A,CO_x} is found to be drastically lowered with catalyst.

In the kinetic model of the catalytic soot oxidation the dependence of E_{A,CO_x} on conversion observed in the loop reactor studies is neglected. A_{CO_x} and E_{A,CO_x} are taken as free parameters in the fitting procedure. Fig. 8 demonstrates that the calculated data cover the experimental curves well; just the maximum CO_x concentration is predicted to be slightly lower (approx. 15%). The apparent activation energy is estimated to be 78 kJ/mol that is not far from the initial value in the loop reactor experiments (56 kJ/mol). This slight difference might be attributed to local gradients in the TPO studies, particularly in temperature range in which soot oxidation is substantially accelerated. In contrast to that, significant gradients are eliminated in the loop reactor. Moreover, the calculated value of 78 kJ/mol suggests that the catalytic reaction is not restricted by surface diffusion as observed in the loop reactor studies. It is speculated that this effect is due to the temperature programmed experiment, i.e. dynamic increase in temperature, and possible hot spots potentially existing in TPO. Furthermore, A_{CO_x} is slightly lower for catalytic reaction than without catalyst.

3.5. Global kinetic modelling of catalytic and non-catalytic soot/NO_x/O_2 reaction

The TPO studies of the catalytic and non-catalytic soot/NO_x/O_2 reaction have been recently reported in detail [9] and therefore

Table 3
Total molar amounts of CO, CO_2, N_2 and N_2O formed in TPO as well as corresponding temperature at peak CO_2 concentration (T_m)[a]

	$n(N_2)$ (μmol)	$n(N_2O)$ (μmol)	n(CO) (mmol)	$n(CO_2)$ (mmol)	T_m (°C)
Pure soot	28	23	5.4	4.6	580
Fe_2O_3/soot	83	14	0.04	9.96	420

[a] *Conditions*: m(soot) = 0.12 g (10 mmol C), $m(Fe_2O_3)$ = 3.19 g (20 mmol), 500 ppm NO, 6 vol.% O_2, Ar balance, F = 500 ml/min (STP), β = 1.5 K/min.

only a brief summary is given (Table 3). The TPO data show simultaneous production of CO, CO_2, N_2 and N_2O, whereupon the profile of the catalytic conversion is shifted to lower temperatures as shown above for the soot/O_2 reaction. Moreover, iron oxide enhances both deNO_x and selectivity of N_2, while even in presence of the catalyst NO reduction represents a side reaction of soot/O_2 conversion. This is proven by the overall amounts evolved in TPO, i.e. $n(CO_x)/(n(N_2) + n(N_2O))$ is ca. 200 with and about 300 without Fe_2O_3 catalyst. Additionally, accumulation of nitrogen occurs neither on the soot nor the catalyst such that the production of N_2 and N_2O is equal to the consumption of NO. For NO reduction C* sites are necessary that are a subset of the C_f atoms. These specific sites reveal appropriate spatial orientation of the molecular orbitals to form cyclic intermediates and N_2, respectively. The proportion of the C* sites is estimated by transient studies which we have also reported lately [9]. Briefly, in these experiments the soot/O_2 and soot/NO reaction is temporally separated. In the 1st step pure soot is oxidised by O_2 at 560 °C until conversion levels of 30, 50 and 80% are achieved. In the 2nd stage the temperature is linearly risen to 715 °C leading to desorption of CO_x. From this amount of CO_x the reactive C_f sites are estimated as done in the previous section. After complete desorption of CO_x, NO is dosed which is supposed to react with all the C* atoms. Hence, from the conversion of NO the abundance of C* sites is derived, whereas it is taken into account that one NO molecule adsorbs dissociatively on two C* atoms. Fig. 9 shows the estimated molar ratio of C* to C_f sites as a function of the soot conversion indicating that only a minority of the reactive carbon is involved in NO reduction. Based on these data an empirical connection between n(C*) and $n(C_f)$ is deduced which is described by Eq. (17) (R^2 = 0.999). It should be stated that in this equation potential rearrangement processes of the C_f sites

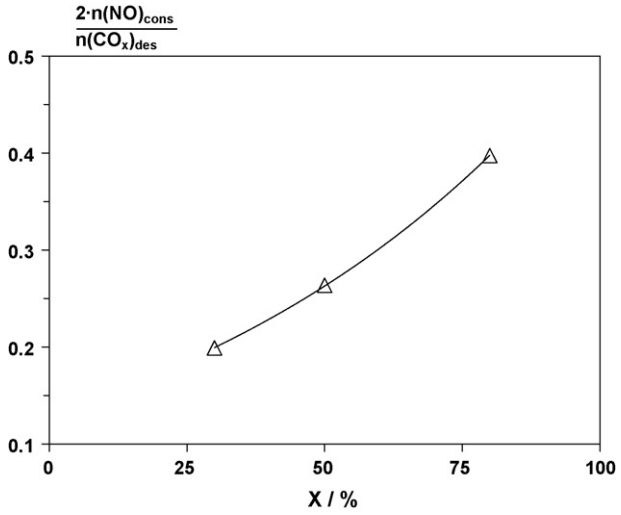

Fig. 9. Estimated number of C* and C_f sites formed in O_2 exposure of the soot. It is assumed that n(C*) corresponds to $2n(NO)_{cons}$, while $n(C_f)$ is equal to $n(CO_x)_{des}$; experimental data refer to a series of transient studies performed with pure soot [9].

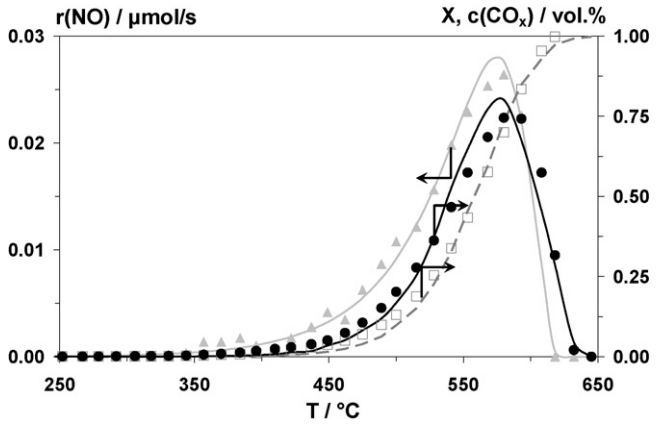

Fig. 10. Comparison of experimental and fitted CO_x concentration (●, —), soot conversion (□, ▬ ▬) and rate of NO reduction (▲, ▬) in non-catalytic soot/NO_x/O_2 reaction; symbols represent experimental data. Conditions and kinetic parameters are listed in Table 5.

Table 4
Experimental and global kinetic parameters of catalytic and non-catalytic soot/O_2 reaction

Parameter	Value	Reference
m_0(soot)	0.12 g (10 mmol C)	
$c(O_2)$	6.0 vol.% (2.5 mol/m^3)	
F	500 ml/min (STP)	
β	1.5 K/min	
λ	8.7 µmol/m^2	This work (TPD experiments)
n_{O_2}	1	[18]
Soot/O_2 reaction		
E_{A,CO_x}	115 kJ/mol	This work (loop reactor experiments)
A_{CO_x}	7.3×10^4 m^3/(mol s)	This work (calculated)
R^2	0.998	
Catalytic soot/O_2 reaction on Fe_2O_3 ($m(Fe_2O_3)$ = 3.19 g (20 mmol)		
E_{A,CO_x}	78 kJ/mol	This work (calculated)
A_{CO_x}	2.5×10^3 m^3/(mol s)	This work (calculated)
R^2	0.999	

are not accounted.

$$n(C*) = 0.13\, e^{(1.4X)} n(C_f) \quad (17)$$

Combination of Eq. (17) with Eq. (3) leads to the following expression for the rate of NO consumption:

$$r(NO) = A_{NO}\, e^{(-(E_{A,NO}/RT))} 0.13\, e^{(1.4X)} n(C_f) c(NO)^{n_{NO}} \quad (18)$$

Eq. (18) does not consider the soot oxidation by NO_2 since under present conditions nitrogen dioxide does not affect soot oxidation and deNO_x effectively [9]. For the non-catalytic soot/NO_x/O_2 conversion the kinetic parameters A_{CO_x} and E_{A,CO_x} are taken from the soot/O_2 reaction, while $E_{A,NO}$ and A_{NO} are fitted. As our mechanistic model involves catalytic effect of Fe_2O_3 in soot/O_2, but not in soot/NO reaction $E_{A,NO}$ determined for the non-catalytic conversion is adopted for the catalytic reaction. Moreover, in the catalytic reaction A_{CO_x}, E_{A,CO_x} and A_{NO} are calculated.

Figs. 10 and 11 show that the calculated curves fit the experimental data of the catalytic and non-catalytic soot/NO_x/O_2 conversion well (Table 5). For NO reduction without catalyst the fit procedure leads to an apparent activation energy of 56 kJ/mol. This value is exactly the same as reported from Yang et al. [49] for the initial soot/NO reaction in the range from 600 to 800 °C. These authors attribute the apparent activation energy to the dissociative adsorption of NO on active carbon atoms. However, in the steady state Yang determines E_A as 161 kJ/mol, which is referred to the decomposition of the surface complexes originated from NO adsorption. Contrary, for the mentioned temperature regime same authors also report on stationary E_A values of 44 kJ/mol [50], 78 and 97 kJ/mol [10].

Furthermore, k_{CO_x} is almost equal to that calculated for the soot/O_2 reaction indicating the reliable estimation procedure. Additionally, A_{NO} is determined to be one order of magnitude higher for catalytic than for non-catalytic soot/NO reaction. This indicates the higher rate of NO reduction in presence of the Fe_2O_3 catalyst, i.e. the acceleration of formation of C* sites. Moreover, the kinetic parameters for catalytic and non-catalytic soot/O_2 reaction hardly change in presence of NO_x. This substantiates that the relatively small amount of NO_x does not affect the soot/O_2 reaction under present conditions.

The TPO profiles (Figs. 7, 8, 10 and 11) as well as respective correlation coefficients (Tables 4 and 5) indicate precise reproduc-

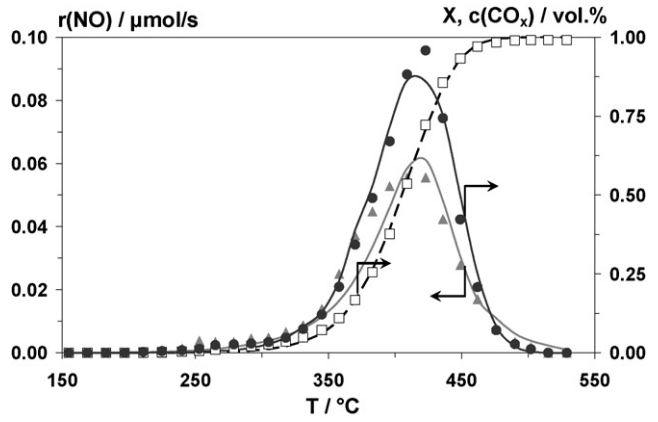

Fig. 11. Comparison of experimental and fitted CO_x concentration (●, —), soot conversion (□, ▬ ▬) and rate of NO reduction (▲, ▬) in catalytic soot/NO_x/O_2 reaction on Fe_2O_3; symbols represent experimental data. Conditions and kinetic parameters are listed in Table 5.

Table 5
Experimental and global kinetic parameters of catalytic and non-catalytic soot/NO_x/O_2 reaction

Parameter	Value	Reference
m_0(soot)	0.12 g (10 mmol C)	
c(NO)	500 ppm (21 mmol/m^3)	
$c(O_2)$	6.0 vol.% (2.5 mol/m^3)	
F	500 ml/min (STP)	
β	1.5 K/min	
λ	8.7 µmol/m^2	This work (TPD experiments)
n_{NO}	1	[10]
n_{O_2}	1	[18]
Soot/NO_x/O_2 reaction		
$E_{A,NO}$	56 kJ/mol	This work (calculated)
A_{NO}	61 m^3/(mol s)	This work (calculated)
R^2	0.966	
E_{A,CO_x}	115 kJ/mol	This work (taken from Table 4)
A_{CO_x}	7.2×10^4 m^3/(mol s)	This work (calculated)
R^2	0.998	
Catalytic soot/NO_x/O_2 reaction on Fe_2O_3 ($m(Fe_2O_3)$ = 3.19 g (20 mmol)		
$E_{A,NO}$	56 kJ/mol	This work (taken from non-cat. reaction)
A_{NO}	824 m^3/(mol s)	This work (calculated)
R^2	0.919	
E_{A,CO_x}	85 kJ/mol	This work (calculated)
A_{CO_x}	1.8×10^4 m^3/(mol s)	This work (calculated)
R^2	0.999	

tion of the experimental traces by the estimation procedure. However, it has to be stated that the reproducibility of the TPO examinations is within a range of about 10%. Thus, in the calculations a slight variation of kinetic parameters is required to obtain an optimum fit for every single experiment. Taking into account this feature an accuracy of ±10% is estimated for all the calculated parameters listed above.

3.6. Model validation

For validation of the kinetic model some TPO studies are simulated, whereupon each result is compared with its corresponding experiment. The following experiments are considered as examples: non-catalytic soot/O_2 reaction with significantly lower mass of soot (0.012 g), catalytic soot/NO_x/O_2 conversion with lower soot mass (0.096 g) and increased O_2 content (10 vol.%) as well as with standard soot mass and higher O_2 content (14 vol.%). The remaining reaction conditions are the same as demonstrated in Tables 4 and 5, respectively. Simulations are carried out based upon Eqs. (16) and (18), using kinetic parameters that are in the 10% reliability interval. Fig. 12 shows that the simulations describe the experimental data well thus validating the kinetic model, although the simulated NO reduction rates are slightly shifted to higher temperatures.

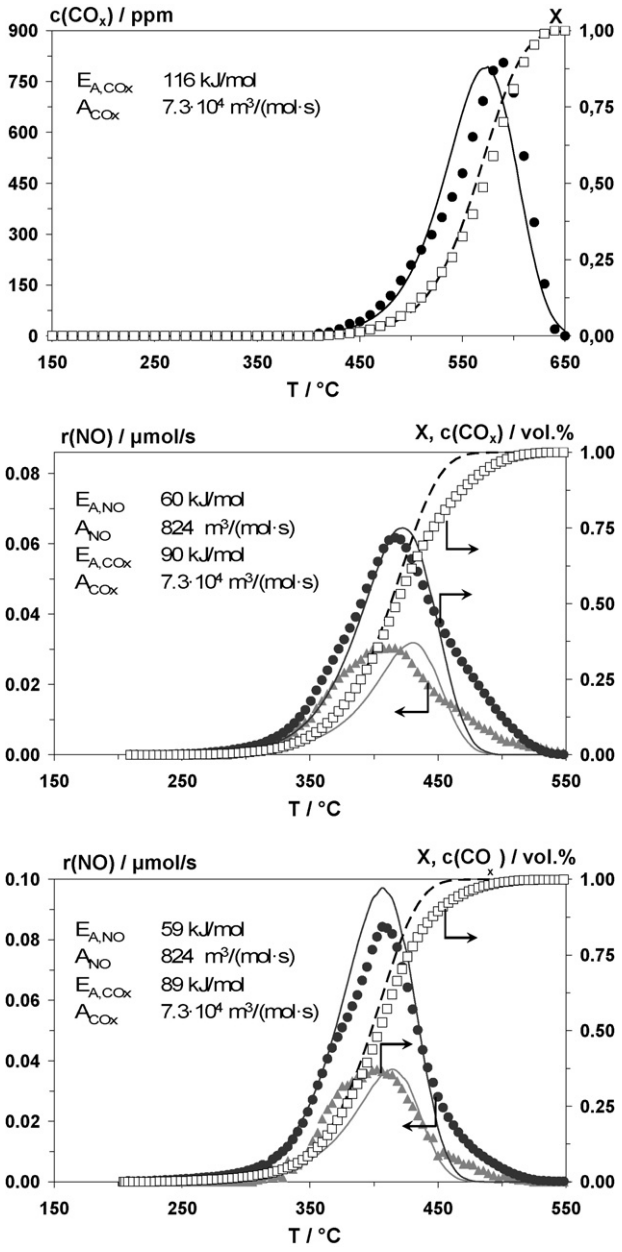

Fig. 12. Comparison of experiment and simulation of non-catalytic soot/O_2 reaction with initial soot mass of 0.012 g (top), catalytic soot/NO_x/O_2 reaction with initial soot mass of 0.096 g and O_2 content of 10 vol.% (middle) and catalytic soot/NO_x/O_2 reaction with standard initial soot mass and O_2 content of 14 vol.% (bottom); remaining parameters are listed in Tables 4 and 5, respectively. CO_x concentration (●, —), soot conversion (□, ▬ ▬) and rate of NO reduction (▲, ▬); symbols represent experimental data.

4. Conclusion

In present work we have constructed a global kinetic model for the catalytic soot/NO_x/O_2 conversion into N_2 and CO_2 on Fe_2O_3. This kinetic model consists of a global rate law for the CO_x formation and for the NO reduction, whereas both equations are coupled by the number of reactive C_f sites. Additionally, the model includes the evolution of the surface area and quantitative connection between C_f and C^* atoms being a subset of the C_f atoms. Furthermore, three different types of kinetic studies were made to build up a broad experimental base and to obtain some independent kinetic parameters. Remaining kinetic parameters were calculated in the fit procedure. The results of the kinetic modelling and validating simulations provide reliable reproduction of the experimental data thus proving substantial consistence between the mechanistic and kinetic model of the soot/NO_x/O_2 reaction on Fe_2O_3 catalyst.

References

[1] M.V. Twigg, Appl. Catal. B 70 (2007) 2.
[2] G. Eigenberger, Chem. Ing. Tech. 77 (2005) 1333.
[3] K. Itoh, T. Tanaka, S. Hirota, K. Kimura, K. Nakatani, EP 1,172,532.
[4] L. Castoldi, R. Mataresse, L. Lietti, P. Forzatti, Appl. Catal. B 64 (2006) 25.
[5] F. Kapteijn, A.J.C. Mierop, G. Abbel, J.A. Moulijn, J. Chem. Soc., Chem. Commun. 16 (1984) 1085.
[6] Y. Teraoka, K. Nakano, S. Kagawa, W.F. Shangguan, Appl. Catal. B 5 (1995) L181.
[7] S. Kureti, K. Hizbullah, W. Weisweiler, Appl. Catal. B 3 (2003) 281.
[8] T. Grzybek, M. Rogoz, H. Papp, Catal. Today 90 (2004) 61.
[9] D. Reichert, H. Bockhorn, S. Kureti, Appl. Catal. B 80 (2008) 248.
[10] J. Yang, G. Mestl, D. Herein, R. Schlögl, J. Find, Carbon 38 (2000) 729.
[11] T. Suzuki, A. Tomita, Ind. Eng. Chem. Res. 33 (1994) 2840.
[12] J.A. Moulijn, F. Kapteijn, Carbon 33 (1995) 1155.
[13] T. Kyotani, A. Tomita, J. Phys. Chem. B 103 (1999) 3434.
[14] G. Mul, F. Kapteijn, C. Doornkamp, J.A. Moulijn, J. Catal. 170 (1998) 258.
[15] H. Teng, E.M. Suuberg, J.M. Calo, Energy Fuels 6 (1992) 398.
[16] J.P.A. Neeft, T.X. Nijhuis, E. Smakman, M. Makkee, J.A. Moulijn, Fuel 76 (1997) 1129.
[17] F. Jacquot, V. Logie, J.F. Brilhac, P. Gilot, Carbon 40 (2002) 335.
[18] B.R. Stanmore, J.F. Brilhac, P. Gilot, Carbon 39 (2001) 2247.
[19] R.H. Hurt, B.S. Haynes, Proc. Combust. Inst. 30 (2005) 2161.
[20] K.J. Hüttinger, in: Y. Yürüm (Ed.), Transport and Other Effects in Coal Gasification, vol. XII, Kluwer-Verlag, Dordrecht, 1988, pp. 453–480.
[21] S.K. Bhatia, D.D. Perlmutter, J. Am. Inst. Chem. Eng. 26 (1980) 379.
[22] S. Reyes, K.F. Jensen, Chem. Eng. Sci. 41 (1986) 333.
[23] P. Balle, H. Bockhorn, B. Geiger, N. Jan, S. Kureti, D. Reichert, T. Schröder, Chem. Eng. Process. 45 (2006) 1065.
[24] D.E. Mears, Ind. Eng. Chem. Process. Des. Dev. 10 (1971) 541.
[25] M. Baerns, H. Hofmann, A. Renken, Chemische Reaktionstechnik, Thieme, Stuttgart, 1991.
[26] P. Chambrion, T. Kyotani, A. Tomita, Energy Fuels 12 (1998) 416.
[27] T. Finke, M. Hartmann, M. Gernsbeck, U. Eisele, C. Vincent, S. Kureti, H. Bockhorn, Thermochim. Acta 473 (2008) 32.
[28] M. Crocoll, S. Kureti, W. Weisweiler, J. Catal. 229 (2005) 480.
[29] B. Feng, S.K. Bhatia, Chem. Eng. Sci. 55 (2000) 6187.
[30] S. Wagloehner, D. Reichert, D. Leon-Sorzano, P. Balle, B. Geiger, S. Kureti, submitted for publication.
[31] R. Vonarb, A. Hachimi, E. Jean, D. Bianchi, Energy Fuels 19 (2005) 34.
[32] S. Ahmed, M.H. Back, Carbon 23 (1985) 513.
[33] D. Reichert, Ph.D. thesis, University of Karlsruhe, 2008.
[34] K. Otto, M.H. Sieg, M. Zinbo, L. Bartosiewicz, SAE Paper 800336.
[35] Ullmanns Encyklopädie der technischen Chemie, vol. 14, VCH, Weinheim, 1977.

[36] O. Hinrichsen, F. Rosowski, M. Muhler, G. Ertl, Stud. Surf. Sci. Catal. 109 (1997) 389.
[37] O. Hinrichsen, A. Hornung, M. Muhler, Chem. Eng. Technol. 22 (1999) 1039.
[38] Z. Du, A.F. Sarofim, J.P. Longwell, Energy Fuels 4 (1990).
[39] K. Sendt, B.S. Haynes, J. Phys. Chem. A 109 (2005) 3438.
[40] S. Haydar, C. Moreno-Castilla, M.A. Ferro-Garcya, F. Carrasco-Maryn, J. Rivera-Utrilla, A. Perrard, J.P. Joly, Carbon 38 (2000) 1297.
[41] G. Barco, A. Marranzano, G. Ghigo, M. Causa, G. Tonachini, J. Chem. Phys. 125 (2006) 194706.
[42] P.W. Atkins, Physical Chemistry, Oxford University Press, 1990.
[43] E.A. Jarvis, A.M. Chaka, Surf. Sci. 601 (2007) 1909.
[44] F. Atamny, J. Blöcker, A. Dübtzky, H. Kurt, O. Timpe, G. Loose, W. Mahdi, R. Schlögl, Mol. Phys. 76 (1992) 851.
[45] I.W. Smith, Fuel 57 (1978) 409.
[46] K. Sendt, B.S. Haynes, Combust. Flame 143 (2005) 629.
[47] K. Sendt, B.S. Haynes, J. Phys. Chem. C 111 (2007) 5465.
[48] K. Sendt, B.S. Haynes, Proc. Combust. Inst. 24 (1992) 1199.
[49] J. Yang, G. Mestl, D. Herein, R. Schlögl, J. Find, Carbon 38 (2000) 715.
[50] J. Yang, E. Sanchez-Cortezon, N. Pfänder, U. Wild, G. Mestl, J. Find, R. Schlögl, Carbon 38 (2000) 2029.